PHYSICAL REVIEW E **74**, 045401(R) (2006)

Coherence-based transverse measurement of synchrotron x-ray radiation from relativistic laser-plasma interaction and laser-accelerated electrons

R. C. Shah,[1,*] F. Albert,[1] K. Ta Phuoc,[1] O. Shevchenko,[1] D. Boschetto,[1] A. Pukhov,[2] S. Kiselev,[2] F. Burgy,[1] J.-P. Rousseau,[1] and A. Rousse[1]

[1]*Laboratoire d'Optique Appliquée, ENSTA, CNRS UMR7639, Ecole Polytechnique, Chemin de la Hunière, 91761 Palaiseau, France*

[2]*Institut fur Theoretische Physik I, Heinrich-Heine-Universität, 40225 Dusseldorf, Germany*

(Received 12 June 2006; published 17 October 2006)

We observe Fresnel edge diffraction of the x-ray beam generated by the relativistic interaction of a high-intensity laser pulse with He gas. The observed diffraction at center energy 4.5 keV agrees with Gaussian incoherent source profile of full-width-half-maximum (FWHM) < 8 μm. Analysis indicates this corresponds to an upper limit on the transverse profile of laser-accelerated electrons within the plasma in agreement with three-dimensional, particle-in-cell results (FWHM=4 μm).

DOI: 10.1103/PhysRevE.74.045401 PACS number(s): 41.50.+h, 41.60.−m, 41.75.Jv, 42.25.Fx

Laser-based approaches towards femtosecond x-ray source development garner much emphasis because of their ability to retain the order of the driving femtosecond light pulses while presenting a compact and economical solution [1]. The research recently reached a new milestone: a narrow divergence (50 mrad), broad-spectrum keV energy x-ray beam generated from the interaction of an intense laser pulse ($I \geqslant 10^{18}$ W/cm^2) with a gas target [2]. At these intensities, the laser plows electrons from its path and generates a longitudinal plasma oscillation that can accelerate both thermal and quasimonochromatic electron beams to several hundred MeV energies [3]. The order 10^9 x-ray photons originate from the transverse oscillations, or betatron motions, of laser-accelerated electrons within the plasma-accelerating structure. Three dimensional particle-in-cell (3-D PIC) simulations show how the acceleration and radiation of the electrons optimize when the laser pulse duration and transverse dimension resonantly match the plasma density [4]. In this regime, a spherical cavitation of the electron density immediately follows the laser pulse. Transversally, the energetic electrons find conditions resembling an ion channel that creates radial restoring force $F = m\omega_p^2 r/2$, where r refers to the electron's radius from the axis [5]. At the electronic densities used for the laser-plasma acceleration (10^{19} cm^{-3}), the tight radius of curvature of the transverse motions, or betatron oscillations, results in broad spectrum, multi-keV synchrotron radiation. The amplitude of each electron's oscillation as well as its energy determine its radiation spectrum.

Because the electrons radiate x-rays incoherently in the betatron mechanism, the x-ray source size determines the correlation, or degree of spatial coherence, between transversely differing points of the emitted radiation. The spatial distribution and energy of the radiating electron beam determine the x-ray source size. Accurate source size measurement characterizes the betatron radiation for coherence based techniques such as phase contrast imaging and holography. The measurement also contains information about the few micrometer transverse distribution of energetic electrons within the laser-plasma accelerator.

At conventional accelerators the intimate connection between the x-ray and electron beam source sizes has led to the use of optical and x-ray diagnostics of the transverse electron beam size. Electron dimensions of order 10–100 μm have been measured by direct imaging and coherence measurements of visible synchrotron light [6]. Hard x-rays generated at synchrotrons have been imaged directly [7], observed with pinhole cameras [8], and interferometrically characterized [9] to measure the electron source dimensions. Thomson scattering from a tightly focused laser pulse has also been used to extract transversal and angular properties of accelerator electrons [10]. Coherence measurements have also characterized laser-based short wavelength sources: high-harmonic radiation in the VUV wavelengths [11], and hard x-ray K shell emission [12]. In the case of the laser synchrotron radiation, the visible and low order components may be contaminated by other radiative processes, and stability as well as repetition rate exclude high accumulation, narrow-bandwidth experiments.

Both the need to increase throughput of the diffracting aperture and support a large bandwidth ($>100\%$) can be addressed by considering the Fresnel diffraction zone. Numerical fitting, with an assumed profile, serves in the place of a direct analytic inversion between the diffraction and the source profile. This Rapid Communication presents measurement of the Fresnel single edge diffraction from the synchrotron x-rays generated from the relativistic laser-plasma interaction at center energy 4.5 keV. The correspondingly fit source size shows only slight sensitivity within reasonable assumptions of the source intensity profile, and the analysis indicates it serves as an upper limit of the transverse profile of laser-accelerated electrons within the plasma, in agreement with 3-D PIC results.

The experiments were performed at the Laboratoire d'Optique Appliquée using a 10 Hz repetition 820 nm titanium-doped sapphire laser [13]. The chirped pulse amplification system delivered energies up to 1 J on target in 30 fs with horizontal polarization. An $f/18$ off-axis parabolic mirror focused the pulse into the helium output of a 3 mm jet providing electronic density 1×10^{19} electrons/cm^3. The laser distribution in the focal plane was Gaussian with waist 18 μm containing 50% of the total laser energy producing

*Electronic address: rahul.shah@ensta.fr

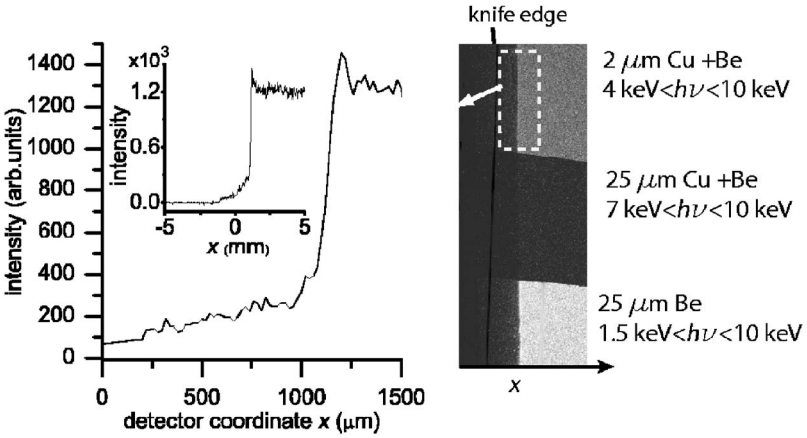

FIG. 1. Single shot x-ray CCD image shows direct x-ray beam (optic-free geometry) divided by filters. The plot at left shows the vertical average of the detected signal in the region filtered by the 2 μm Cu while inset shows larger extent.

vacuum intensity 3×10^{18} W/cm^2. These conditions match those of the previous Letter. The energetic electrons were deflected by a 1 T, 10 cm permanent magnet onto a fluorescent screen providing an electron spectrum for energies between 40–200 MeV. The steel edge vertically bisected the x-ray beam 13 cm from laser focus, and a cooled charge-coupled device (CCD) of 20 μm pixels detected the x-ray signal on axis 195 cm from the blade. 25 μm Be filter, permitting photons >1 keV, filtered the entire CCD. Two additional Cu filters, one of 2 μm and the other 25 μm, selected photons primarily above 4 keV and 7 keV respectively within each shot.

An example of the observed x-ray signal is presented in Fig. 1 along with the raw intensity profile obtained by averaging the image perpendicular to the knife shadow within the region filtered by the Be and 2 μm Cu filter combination. In the inset of 1 cm extent, the signal clearly distinguishes from noise, and the principal plot indicates a pattern near the edge differing from lower frequency variations. Vertical averaging of the bottommost, Be only region, reveals a similar intensity profile, characteristic of Fresnel edge diffraction. In the most heavily filtered region, the signal is too weak and the photon noise dominates. From shot to shot, the diffraction pattern fluctuated in position over approximately 200 μm on the detector corresponding to x-ray source fluctuations of the order of the laser focal spot. Five pixels span the primary oscillation (100 μm) above the plateau intensity outside the shadow.

Within the plasma channel, all the radiating electrons oscillate around one unique central axis due to the Coulomb restoring force of the ions, and the electrons radiate significantly only at the peaks of their transverse oscillations [14]. The radiation from individual betatron oscillation peaks of a single electron can be summed incoherently since, in the synchrotron regime, such interference averages rapidly over small bandwidths as well as with consideration of slightly differing electron energies. Because the synchrotron emission emits from a near light speed particle on a curved trajectory, the wavefront becomes asymmetric. In lieu of the actual source, a spherical wave emitter displaced from the oscillation axis by $\rho/2\gamma^2$, where ρ is the electron's radius of curvature and γ its relativistic factor, simplifies analysis [15]. In the laser-plasma wiggler, $\rho[\mu\text{m}]\sim10\gamma$ yields a submicrometer displacement.

As no detailed spectral measurement yet exists for this source, the measured single shot spectral information was quantified by fitting an exponentially decaying radiation power spectrum of variable decay constant such that its integrated product with the x-ray filter [16] and CCD responses corresponded with the measured intensity ratio between spectrally proximal filters (bands). For the spectral form $\frac{dI}{d\omega}=e^{-E_p/E_d}$, where E_p [keV] refers to photon energy, this yielded a piecewise spectrum with decay constant of $E_d=3.7\pm0.4$ keV when fit to the ratio between the most-accepting (Be) and midfilter (2 μm Cu) and $E_d=14.2\pm1$ keV for the fit with the mid- and most-restrictive filter (25 μm Cu). Limited crystal spectroscopy shows agreement with a sharp initial drop in the vicinity of 1 keV and low intensity plateau to higher energies.

The slow, nearly linear intensity rise in the shadow region observed in the raw data (Fig. 1) closely resembles previous synchrotron-based experimental studies showing finite transmission effects in edge diffraction of highly absorbing materials [17]. In this research, the wedge shaped knife diffraction edge with apex thickness ~10 μm allows transmission effects between 5–7 keV. To accurately describe the observations, the analysis includes the phase and absorption effects of the iron wedge [16] in calculation of the diffraction from the Fresnel approximation of the Fresnel-Kirchhoff integral [18]. Figure 2 presents these calculated results given the experimental distances for an exemplary monochromatic and the two broad spectrum cases. The calculated result for the 5 keV radiation shows the transmissivity creates a slow pedestal in addition to the peaking in intensity characteristic of Fresnel edge diffraction; the ideal knife edge (not shown) shows a few percent greater contrast at this energy. The inset of Fig. 2 shows the contributing relative power spectrum for the two assumed radiation spectra. Because of the combined filtering of the CCD (high frequency side) and Cu (low frequency side), the spectra change only slightly, and the calculated diffraction patterns change almost indiscernibly. Within the bounds of the 2 μm Cu and 25 μm Be filter combination, the two differing exponentials are taken to span the true source spectrum to sufficient accuracy for the observed diffraction. Most significantly, the broad spectrum eliminates almost completely the higher order oscillations. In comparison, calculations with an ideal knife edge over these broad spectra show nearly identical results with the exception of

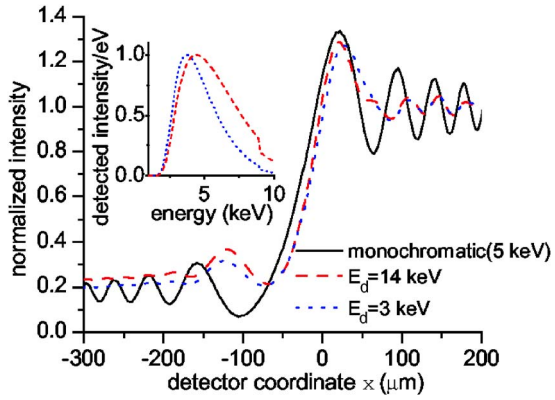

FIG. 2. (Color online) Calculated diffraction for monochromatic spectrum and the detected spectrum in the case of the two limiting source spectrum estimates. Inset shows detected power spectrum for the two source spectra.

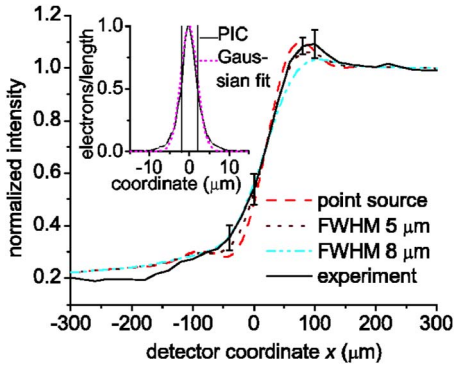

FIG. 4. (Color online) Averaged experimental diffraction result (error bars correspond to standard deviation) and theoretical curves for Gaussian source intensity profiles. Inset shows linear distribution of accelerated electrons with energy >100 MeV obtained from PIC simulation (dashed line indicates FWHM).

the transmission pedestal in the knife shadow. Changes over a broad range of transmission parameters (wedge slope and apex thickness) show significant changes only in the knife shadow region.

An appropriate radiation intensity profile stems from the characteristics of the betatron radiation mechanism in conjunction with reasonable estimates of the electron beam. The transverse self-injection of electrons into the accelerating bubble-like structure suggests a full range of transverse oscillation amplitudes of the radiating electrons. Neglecting effects of laser polarization on the injection and distribution of the electrons, the profile adopts cylindrical symmetry. The radiated intensity of each electron peaks near its critical energy $\hbar\omega_c[\mathrm{eV}]=5\times10^{-21}\gamma^2 n_e[\mathrm{cm}^{-3}]r_0[\mu\mathrm{m}]$ where γ is the electron relativistic factor, n_e the electronic plasma density, and r_0 the electron's transverse oscillation amplitude. Beyond this energy, the radiated intensity falls exponentially. Since ω_c varies linearly with r_0, the radiated intensity of synchrotron x-rays drops on-axis. Figure 3 shows how the extent of this modulation depends on the relationship between the radiation frequency ω and ω_c of the bulk of the

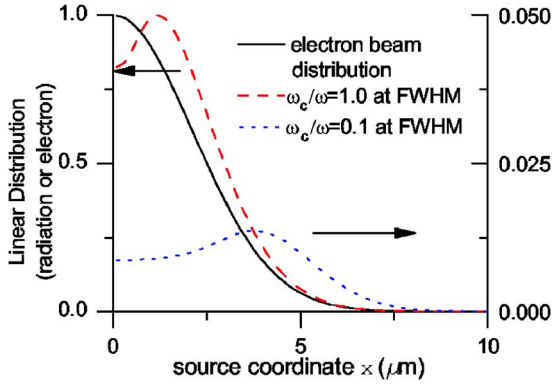

FIG. 3. (Color online) Calculated radiation profiles at photon energy 4 keV from the betatron mechanism for monochromatic, Gaussian electron transverse distribution of FWHM=5 μm (solid) corresponding to oscillation amplitudes. Radiation profile, projected onto one Cartesian coordinate, is presented for ~25 MeV (dotted) and near 100 MeV (dashed) electrons.

electron beam. Here, to rest within the order of parameters of interest, the electron transverse distribution function is taken to be Gaussian of FWHM=5 μm, and this distribution is taken to provide the maximum oscillation amplitude of each electron. For two different representative electron beam energies, 25 MeV (dotted line) and 100 MeV (dashed line), the resulting betatron radiation at 4 keV is calculated from analytical expression for each electron in this transverse profile at ionic density of the interaction. The radiated intensity is integrated along one Cartesian coordinate to generate the intensity profile perpendicular to the knife edge. For the lower energy beam, with $\omega_c/\omega=0.1$ at r_0=FWHM/2, the radiated intensity drops one hundred fold with respect to the higher energy beam. Moreover, the radiated profile widens by roughly a factor two with respect to the responsible electron distribution since the higher values of r_0 compensate the low beam energy. In contrast, the intensity profile of the ~100 MeV beam, with $\omega_c/\omega=1$, nearly matches that of the electrons. As the on-axis synchrotron power spectrum rests relatively flat for frequencies as small as $0.1\omega_c$, consideration of higher energy electrons increases the agreement between the electron and intensity distributions. This trend was observed in calculation with a uniform electron profile as well, and, in this sense, the determined radiation source profile represents an upper limit of an average electron beam spread within the plasma.

Close inspection of the experimental images evidences small perturbations in the quality of the edge. Quantification, by analysis of each horizontal image line, shows a near normal edge distribution of FWHM=4 pixels with respect to a true line. Figure 4 presents the result of alignment and averaging over five shots along with theoretical curves that include the effects of detected power spectrum, Gaussian cross-sectional intensity profiles, and the blurring incurred by vertical averaging over the edge perturbations. The edge quality prevents determination of the lower limit while differentiation of the fringe visibility establishes as the upper limit the theoretical curve for the 8 μm FWHM. Comparison of theoretical curves with and without the edge effects shows no change in this determination of the upper limit, a result of the more significant source blurring at this size. The high

resolution observed results from the asymmetric peaking of the pattern, the width of which can be estimated from simple optical path length arguments as $\sim\sqrt{\lambda D}$, where D is the distance between the diffraction plane and detector [19]. The resolution of the source size reaches order of micrometers for the 20× magnification. Calculation of the theoretical diffraction with the slightly modulated Gaussian intensity profile derived from the Gaussian electron distribution with $\omega_c/\omega \geqslant 1$ (Fig. 3) for these values of FWHM produces near identical curves. The approach appears relatively insensitive to profile: use of the uniform transverse electron beam profile does not change the determined upper limit on source dimension. Even with r_0 of the electrons equal to 2 μm, an electron energy of only 100 MeV is necessary for critical radiation energy of 4 keV, in accord with the measured broad distribution of electron energies.

The relativistic laser-plasma interaction under these experimental conditions has been previously modeled using a supercomputer based 3D PIC simulation [20]. These results have shown quantitative agreement with experimental measurements of the x-ray spectrum, electronic-density dependence, and electron beam spectrum. The inset of Fig. 4 presents the simulation result of the transverse beam profile of electrons at the plasma exit, with energy greater than 100 MeV, along the laser polarization (corresponding to the perpendicular to the diffraction edge in the experiment). The 4 μm FWHM of the near Gaussian distribution falls within the upper limit set by the Fresnel diffraction based measurement, and within the ion-channel where the synchrotron mechanism occurs, the non-Gaussian wings in the PIC result contain only a few percent of the total charge. The few micrometer dimension of the laser-accelerated electrons contrasts with the relatively large ~20 μm diameter of the ion channel observed in simulation. Consideration of the simultaneous linear acceleration of the electrons introduces dampening of the transverse motion, and numerical solution of this motion shows that injection even near the edge of the "ion-bubble" results in few micrometer oscillation amplitudes after the electrons reach order 100 MeV.

By analysis of single-edge Fresnel diffraction, the x-ray source size of this fully laser-based synchrotron source has been estimated as Gaussian with FWHM < 8 μm, more than one order of magnitude smaller than at typical third-generation synchrotrons [21]. This corresponds to order 10^{-2} spatially coherent photons/eV across a several keV bandwidth. Improvement of the diffraction edge will increase the precision of the technique. The analysis shows this measurement serves as an upper limit of the transverse dimension of relativistic electrons within the plasma in the near-resonant, highly nonlinear regime of laser-wakefield acceleration, and the result agrees with that of PIC simulation. Such measurements are fundamental to both the x-ray radiation and electron beam emittance, the latter of which betatron oscillations can dominate as opposed to space charge [22].

We acknowledge discussion with G. Mourou. This work was supported by European Community Contract Nos. HPRI-CT-1999-00086, HPRI-CT-2000-40016, and HPRI-CT-1999-50004 (FAMTO project). R.C.S. was supported by CNRS of France and U.S. National Science Foundation (Grant No. 0502281).

[1] R. Service, Science **298**, 1356 (2002).
[2] A. Rousse *et al.*, Phys. Rev. Lett. **93**, 135005 (2004).
[3] J. Faure *et al.*, Nature (London) **431**, 541 (2004); C. Geddes *et al.*, *ibid.* **431**, 538 (2004); S. Mangles *et al.*, *ibid.* **431**, 535 (2004).
[4] A. Pukhov and J. Meyer-ter-vehn, Appl. Phys. B: Lasers Opt. **74**, 355 (2002).
[5] D. H. Whittum, A. M. Sessler, and J. M. Dawson, Phys. Rev. Lett. **64**, 2511 (1990); E. Esarey *et al.*, Phys. Rev. E **65**, 056505 (2002); I. Kostyukov, S. Kiselev, and A. Pukhov, Phys. Plasmas **10**, 4818 (2003).
[6] N. Artemiev, O. Chubar, and A. Valentinov, Proc. EPAC SITGES (Barcelona), p. 340 (1996); T. Tseng *et al.*, Proc. Part. Accel. Conf. (Knoxville), p. 3465 (2005); Y. Takayama and S. Kamada, Phys. Rev. E **59**, 7128 (1999).
[7] T. Weitkamp *et al.*, Nucl. Instrum. Methods Phys. Res. A **467-468**, 248 (2001).
[8] C. Limborg, J. Safranek, and P. Stefan, Proc. EPAC (Vienna), p. 1774 (2000).
[9] V. Kohn, I. Snigireva, and A. Snigirev, Opt. Commun. **198**, 293 (2001).
[10] R. W. Schoenlein *et al.*, Science **274**, 236 (1996).
[11] T. Ditmire *et al.*, Phys. Rev. Lett. **77**, 4756 (1996); R. A. Bartels *et al.*, Science **19**, 376 (2002).
[12] D. Boschetto *et al.*, in *CLEO/QUELS Technical Digest* (Optical Society of America, Washington, DC, 2006), p. CFF2.
[13] M. Pittman *et al.*, Appl. Phys. B: Lasers Opt. **74**, 529 (2002).
[14] J. D. Jackson, *Classical Electrodynamics* (Wiley, New York, 1976).
[15] N. Smolyakov, Nucl. Instrum. Methods Phys. Res. A **405**, 229 (1998).
[16] Center for X-ray Optics (2006), URL http://www-cxro.lbl.gov/.
[17] A. Groso *et al.*, Appl. Phys. Lett. **81**, 4076 (2002); Y. Hwu *et al.*, J. Phys. D **35**, R105 (2002).
[18] M. Born and E. Wolf, *Principles of Optics* (Macmillan, New York, 1964).
[19] G. Margaritondo, *Elements of Synchrotron Light* (Oxford University Press, New York, 2002).
[20] Virtual Laser-Plasma Laboratory PIC code. See Ref. [4].
[21] D. Attwood, *Soft X-rays and Extreme Ultraviolet Radiation* (Cambridge University Press, Cambridge, 1999).
[22] J. S. Humpheries, *Charged Particle Beams* (Field Precision, Albuquerque, 2002).